TISSUE ENGINEERING: Part A
Volume 25, Numbers 7 and 8, 2019

DOI: 10.1089/ten.tea.2018.0142

termis
Tissue Engineering
& Regenerative Medicine
International Society

ORIGINAL ARTICLE

A Functional Tissue-Engineered Synovium Model to Study Osteoarthritis Progression and Treatment

Robert M. Stefani, MSc,[1] Saiti S. Halder,[1] Eben G. Estell, MSc,[1] Andy J. Lee, BEng,[1] Amy M. Silverstein, PhD,[1] Evie Sobczak, BS,[1] Nadeen O. Chahine, PhD,[1,2] Gerard A. Ateshian, PhD,[1,3] Roshan P. Shah, MD, JD,[2] and Clark T. Hung, PhD[1]

Little is known about the critical role of the synovium in joint homeostasis and osteoarthritis (OA). We describe a novel *in vitro* tissue-engineered (TE) model to investigate the structure–function of synovium through quantitative solute transport measures. This TE synovium model was developed using healthy bovine, $CD14^-$ fibroblast-like synoviocytes (FLS, or Type B synoviocytes) encapsulated in a Matrigel scaffold. The bovine system is well established in musculoskeletal research, allowing comparisons to be made to previous work. Sheet-like TE constructs were precultured to attain native protein composition and polarized structure, as determined by immunohistochemistry and confocal microscopy, and subsequently exposed to interleukin-1α (IL) or dexamethasone (DEX). The biological responses, including nitric oxide and hyaluronic acid (HA) secretion, of engineered synovium paralleled that of native synovium. While HA media content increased in response to both IL and DEX, a higher proportion of HA was low molecular weight (<460 kDa) in IL compared to CTL or DEX. Meanwhile, lower permeability of 70 kDa dextran was strongly correlated ($r = 0.9736$, $p = 0.0264$) with a lower ratio of collagen to DNA in TE synovium, a trend that was qualitatively similar to explants (EXPs). Histological staining confirmed similar structural changes to TE and EXP specimens in response to DEX or IL, including intimal hyperplasia and matrix compaction. This suggests that, in addition to inflammation leading to HA breakdown and increased joint clearance, competing factors such as changes in synovium matrix content and permeability to a given solute size are also at play. Moreover, FLS-only engineered tissues, similar in cell composition to healthy native synovium, grew to contain $CD14^+$ macrophage-like synoviocytes (MLS, or Type A synoviocytes) in culture with IL, suggesting the potential role for cell transdifferentiation in the inflammatory response of synovium. Co-culturing FLS with MLS in this model also demonstrated the versatility to reverse engineer healthy and diseased synovium. Through the development of increasingly biofidelic synovium models, key gaps can be filled in our understanding of synovium function in health and OA.

Keywords: synovium, osteoarthritis, *in vitro* models, solute transport

Impact Statement

The synovium envelops the diarthrodial joint and plays a key regulatory role in defining the composition of the synovial fluid through filtration and biosynthesis of critical boundary lubricants. Synovium changes often precede cartilage damage in osteoarthritis. We describe a novel *in vitro* tissue engineered model, validated against native synovium explants, to investigate the structure–function of synovium through quantitative solute transport measures. Synovium was evaluated in the presence of a proinflammatory cytokine, interleukin-1, or the clinically relevant corticosteroid, dexamethasone. We anticipate that a better understanding of synovium transport would support efforts to develop more effective strategies aimed at restoring joint health.

Departments of [1]Biomedical Engineering, [2]Orthopedic Surgery, and [3]Mechanical Engineering, Columbia University, New York, New York.

Introduction

THE SYNOVIUM (Fig. 1) ENVELOPS the diarthrodial joint and plays a key regulatory role in defining the composition of the synovial fluid through filtration (barrier–function)[1] as well as biosynthesis of critical boundary lubricants such as lubricin and hyaluronic acid (HA).[2,3] Characterized by a unique intima/subintima architecture, synovium is distinct from other barrier membranes found in the body.[4] The synovial intima is composed of a dense collagenous matrix (primarily type I and IV)[5] with cells interspersed, lacking a distinct basement membrane.[6]

The normal intimal lining (Fig. 1A), which is in direct contact with the synovial fluid, is about 1–4 cells thick and composed of ~90% fibroblast-like synoviocytes (FLS) and 10% macrophage-like synoviocytes (MLS).[7] The subintimal layer, which is about 5 mm thick in healthy tissue, is relatively acellular and heterogeneous. Depending on the depth and joint location, the extracellular matrix (ECM) consists of a mixture of fibrous and collagenous (type I, III, IV, V, and VI) dense connective tissue regions and adipose.

While synovial inflammation is typically associated with rheumatoid arthritis (RA), it is also a key feature of osteoarthritis (OA).[8] The OA synovium thickens into a pannus-like structure with an increase in cellularity (hyperplasia), fibrosis, vascularity, and innervation (Fig. 1B).[9–12] Multiple reports have linked synovial hyperplasia as well as aberrant production of proinflammatory cytokines to increased cartilage loss in patients with OA[13] and overall progression of joint degeneration.[2,14–16] Many of these changes to the synovium often precede cartilage damage.[17] Changes to the synovial composition likely affect the tissue's ability to regulate clearance in and out of the joint space,[18,19] but the mechanism by which this occurs has not been elucidated.

Despite the growing appreciation for the role that the synovium plays in joint health and pathology, quantitative structure–function data for this tissue remain incomplete. *In vivo* studies utilizing tracer molecules have offered important insights on solute transport across the synovium.[20–22] However, it can be a challenge to resolve mechanisms below the whole-joint level due to the inherent confounding variables of the *in vivo* environment, including ill-defined boundary conditions arising from vasculature throughout the subintima.[18]

Toward gaining a greater understanding of synovium function under more well-defined conditions, investigators have turned to *in vitro* systems, each with relative strengths and weaknesses (Table 1). Synovial explants (EXPs) have the benefit of native ECM and spatial organization of resident FLS and MLS, but availability of ''normal'' clinical specimens is extremely limited. Clinical specimens are typically obtained from advanced-stage OA patients, which can be contaminated with fatty tissue and irregular in geometry, making them difficult to manipulate and perform well-defined functional analyses *in vitro*.[23] Additional variability is introduced due to disease state, donor, and harvest site.[5] As such, the few studies examining synovium EXPs have focused mainly on biological measures.[24,25]

FLS, the primary cells in the synovium, are largely responsible for ECM production[4,26] and lubricant secretion,[27–29] and contribute to the cascade of inflammatory cytokines in OA synovial fluid.[4] Hence, most biological studies of isolated synoviocytes have focused on FLS. This focus is facilitated by high proliferation in two-dimensional monolayers, whereby FLS exclude both the MLS and contaminating blood cells at early passage.[14] These synovium-like monolayers have been cultured on various substrates, including filter membranes,[1,30] temperature-responsive dishes,[31] cartilage EXPs,[32] tissue-engineered (TE) cartilage,[33] and even in suspension.[34,35] However, simple cell layers lack the dense ECM and three-dimensional architecture of the intima and subintima that play an integral role in the function of native tissue.

TE synovium may be able to overcome these limitations. Kiener et al. created an engineered synovium micropellet by encapsulating RA-donor FLS in Matrigel, a scaffold material that shares many ECM constituents with native synovium. These tissues were able to reorganize in an intimal lining

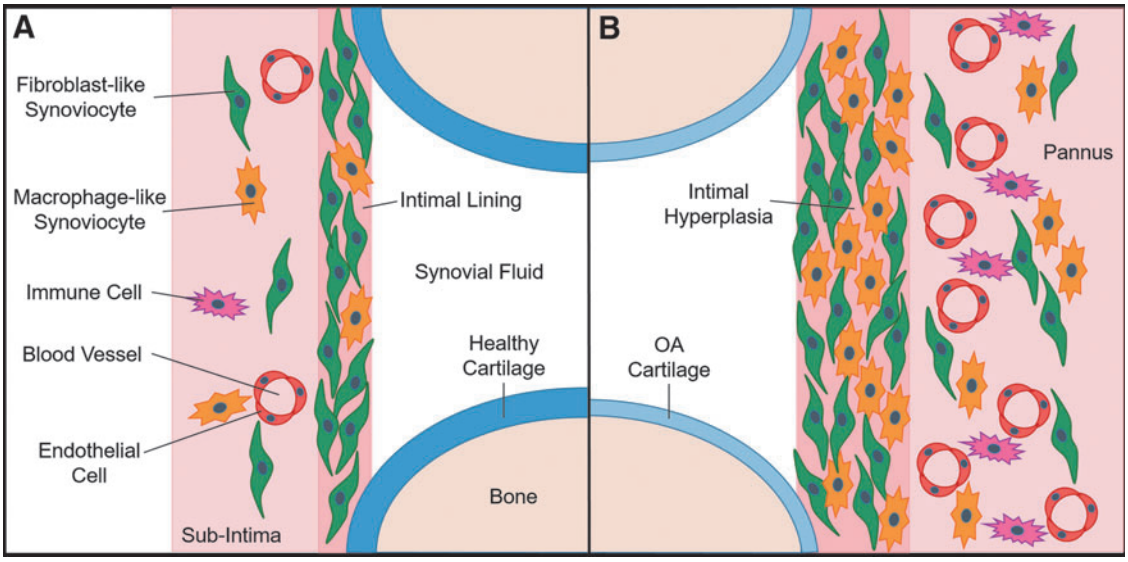

FIG. 1. Relevant synovium anatomy in an idealized knee joint. **(A)** Normal synovium comprises ~90% FLS and ~10% MLS. **(B)** OA synovium composition and structure change dramatically, coinciding with altered secretion of lubricants and inflammatory mediators. OA, osteoarthritis; FLS, fibroblast-like synoviocytes; MLS, macrophage-like synoviocytes.

Table 1. Comparison of *In Vitro* Synovium Models

	Cell monolayer[1]	*TE RA micropellet*[4]	*Native explant*[58,59]	*TE Synovial membrane*
Gross morphology	X	X	✓	✓
Structural organization	X (Pseudo-intima only)	✓ (Intima + subintima)	✓	✓ (Intima + subintima)
ECM content	X	✓	✓	✓
Cell content	X (FLS only)	✓ (FLS ± monocytes)	✓	✓ (FLS ± MLS)
Lubricant secretion	✓	✓	✓	✓
Transport	✓	X	✓	✓
Defined geometry and initial content	✓	✓	X	✓
Clinical specimen availability	✓	✓	X	✓
High-throughput mechanistic studies	✓	✓	X	✓

ECM, extracellular matrix; FLS, fibroblast-like synoviocytes; MLS, macrophage-like synoviocytes; TE, tissue engineered; RA, rheumatoid arthritis.

architecture that became hyperplastic in the presence of tumor necrosis factor-α (TNF-α), as well as secrete lubricin and support blood monocyte survival.[26]

While cellular features of the intima were recapitulated in micropellet culture, this model lacks the geometry and scale to allow quantitative measurements of key synovial functions like regulation of solute transport. We hypothesize that by modifying this system to create a sheet-like, stratified FLS-Matrigel-based engineered synovium, chemical-induced structural and biochemical changes observed in native tissues can be recreated and related to altered solute permeability. Furthermore, the model will provide a platform for adding degrees of complexity (i.e., MLS), which mimic structural changes at different disease states.

Materials and Methods

The TE synovium model was developed using bovine tissue. The bovine system was selected due to the robust and consistent growth exhibited by engineered constructs and ease of procurement of synovial EXPs, which facilitated model validation by comparing engineered and native tissues. Quantitative measurements of engineered tissue were compared to human OA EXPs whenever possible, as the ultimate goal is to model clinical specimens. TE constructs were prepared by encapsulating FLS in Matrigel®[26,36] and allowing gelation directly in a Transwell® to create a flat, disk-shaped construct. TE synovium was compared to native tissue EXPs in the presence of a proinflammatory cytokine, interleukin-1 (IL), which has been implicated in the pathogenesis of cartilage matrix degradation in OA,[37,38] or the clinically relevant corticosteroid drug, dexamethasone (DEX).[39]

First, key features of native synovium structure and protein expression were assessed (Study 1). Tissue behavior was then compared in response to IL or DEX (Study 2). This included lubricant secretion, ECM, and cell content, and for the first time, quantitative measurements of solute transport function. Finally, a strategy for incorporation of MLS with FLS is described to demonstrate the flexibility of the TE synovium model (Study 3).

Synovium EXP harvest

Fresh synovial tissue was harvested from discarded (Institutional Animal Care and Use Committee-exempt) bovine calf knee joints (2–4 weeks old). EXPs were collected from the region adjacent to the medial and lateral femoral condyles. For subsequent *in vitro* experiments, tissue was pooled from four donor animals and diced into consistent $\sim 5\,mm \times 5\,mm$ pieces. Human OA synovium EXPs were collected (IRB #AAAQ2703) from the region adjacent to the medial and lateral femoral condyle of seven subjects (three male and four female) during total knee arthroplasty. The OA grade (out of 4) and age of the patients was 3.6 ± 0.79 (range 2–4) and 69 ± 7.5 years (range 60–80 years), respectively. EXPs were trimmed of excess adipose and outer capsule tissue before dicing. Human tissue was kept separated by donor for experiments.

Formation of TE synovium constructs

Synovium was digested in collagenase type II (Cat. No. LS004177; Worthington Biochemical Corporation) for 2 h with stirring at 37°C. Digested synovial cells were filtered through a 70 μm porous nylon mesh. Viable cells were counted and plated at a density of 1.76×10^3 cells/cm^2 for expansion. The mixed population of primary synovial cells was expanded for two passages in α-Minimum Essential Medium (αMEM, Cat. No. 12000022; ThermoFisher) containing 10% fetal bovine serum (FBS, Cat. No. S11550; Atlanta Biologicals), 1% antibiotic-antimycotic (Cat. No. 15240062; ThermoFisher), and 5 ng/mL fibroblast growth factor-2 (Cat. No. PHG0264; ThermoFisher).[40–42] The resulting population of FLS was suspended at 5×10^6 cells/mL in 7 mg/mL Matrigel (Cat. No. 354234; Corning).

For biochemical and histological analyses, constructs were cast in 6.5 mm Transwells with 3 μm polyester filter membranes (Cat. No. 3472; Corning), resulting in disk-shaped specimens attached to the underlying filter (volume = 100 μL, diameter = 6.48 mm, and thickness = 3.03 mm) (Fig. 2A). Specimen dimensions were calculated based on gel volume and Transwell geometry. Transport analyses were conducted using a parallel set of TE specimens cast in a scaled-down (volume = 25 μL, diameter = 4.27 mm, and height = 1.70 mm) 4.26 mm Transwell system (Cat. No. 3385; Corning).

To induce ECM deposition as well as the stratified intimal/subintimal organization, constructs were initially cultured in Dulbecco's Modified Eagle's Medium (DMEM,

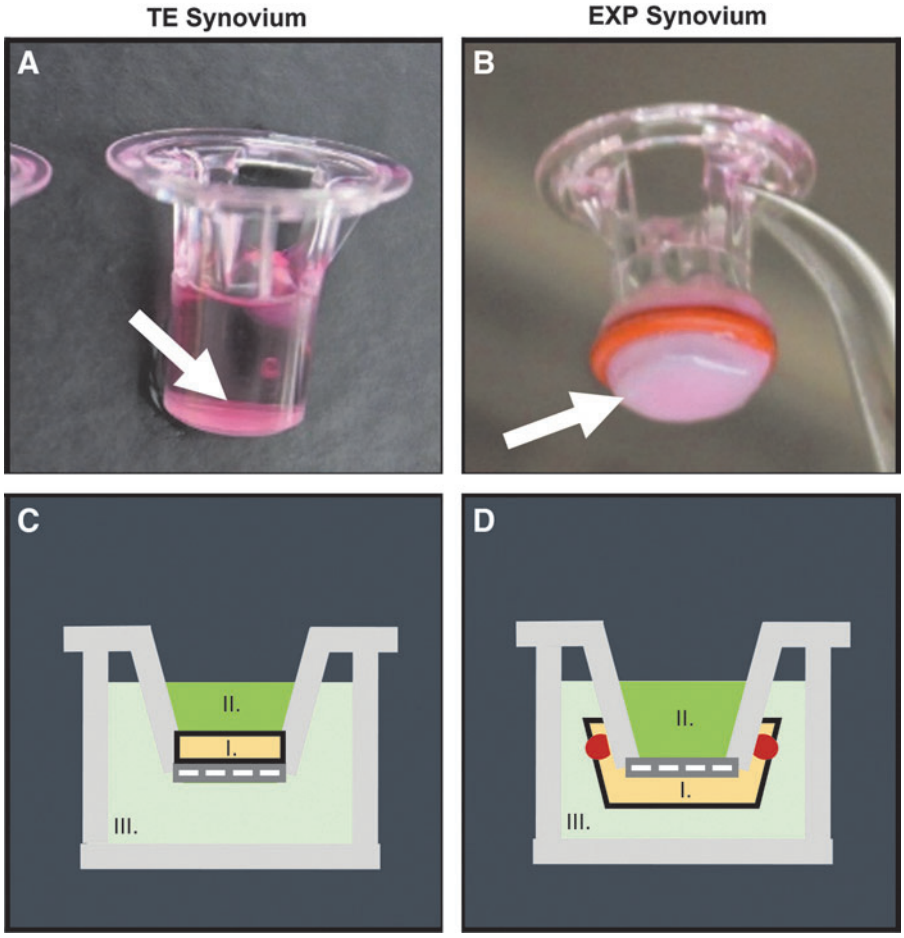

FIG. 2. Changes in permeability of FITC-labeled dextran in synovium were assessed using a Transwell® system. TE synovium **(A, C)** was cultured and tested *in situ* on the top of a 4.26 mm Transwell insert (*arrow*). EXP synovium **(B, D)** was secured to the underside of a 6.5 mm Transwell insert using a rubber gasket for transport measurements (*arrow*). For both tissues (I), the dextran suspension (II) was placed in the luminal compartment (i.e., the synovial cavity). Phosphate-buffered saline (III) was added to the basolateral compartment (i.e., the fibrous capsule and associated vasculature) and sampled at time points to quantify joint clearance. FITC, fluorescein isothiocyanate; TE, tissue engineered; EXP, explant.

Cat. No. 12100046; ThermoFisher) supplemented with 10% FBS, 1% antibiotic–antimycotic, and 50 µg/mL ascorbic acid-2-phosphate (Cat. No. A8960; Sigma) for 21 days in the upper compartment of the Transwell only. During this period, the basolateral compartment was left empty and media in the luminal compartment were changed thrice per week. Luminal media volumes were 100 and 300 µl for 4.26 and 6.5 mm Transwells, respectively.

In vitro *application of proinflammatory cytokine or corticosteroid drug*

TE constructs and EXPs were individually cultured for two weeks in one of three conditions: serum-free basal media (CTL), 100 nM DEX, or 10 ng/mL IL-1α (IL).[39,43] For TE constructs, media were introduced to both luminal and basolateral compartments, and media were changed thrice per week. Basolateral media volumes were 200 and 700 µL for 4.26 and 6.5 mm Transwells, respectively.

Individual EXP specimens were cultured in 1 mL medium each, again with medium changes thrice per week. Human EXPs were cultured in identical conditions, but IL-1α was substituted with IL-1β, as it is a more potent isoform in adult tissues.[44] Basal media consisted of DMEM supplemented with 50 µg/mL L-proline (Cat. No. P5607; Sigma), 100 µg/mL sodium pyruvate (Cat. No. S8636; Sigma), 1% ITS™+ Premix (contains insulin, transferrin, selenous acid, bovine serum albumin, and linoleic acid, Cat. No. 354352; Corning), 1% antibiotic–antimycotic, and 50 µg/mL ascorbic acid-2-phosphate. TE synovium was harvested on day 21 (initial maturity, start of treatment) and day 35 (end of 2-week treatment) for biochemical, histological, and transport analyses. Synovium EXPs were harvested on day 0 (initial harvest, start of treatment) and day 14 (end of 2-week treatment).

Biochemistry

TE constructs ($N = 8–10$), bovine EXPs ($N = 9–10$), and human OA EXPs ($N = 4–7$ replicates per donor) were frozen at −20°C. Lyophilized samples were weighed to obtain specimen dry weight (DW) before digestion. Samples were solubilized by incubating for 16 h at 56°C in 0.5 mg/mL proteinase K (Cat. No. 193504; MP Biomedicals) in 50 mM Tris-buffered saline containing 1 mM ethylenediaminetetraacetic acid, 1 mM iodoacetamide (Cat. No. 12227-1000; Acros), and 10 mg/mL pepstatin A (Cat. No. BP2671100; Fisher).[45] DNA and collagen content were analyzed using the Picogreen (Cat. No. P11496; ThermoFisher) and orthohydroxyproline (OHP) assays, respectively. The OHP assay was performed as previously described.[46]

Media analyses

Hyaluronic acid (HA) and nitric oxide (NO) in the media were quantified using the Hyaluronan Quantikine ELISA Kit (Cat. No. DHYAL0; R&D Systems) and Griess Reagent Kit (Cat. No. G7921; ThermoFisher), respectively. To account for variations in size of the specimens, HA values were normalized

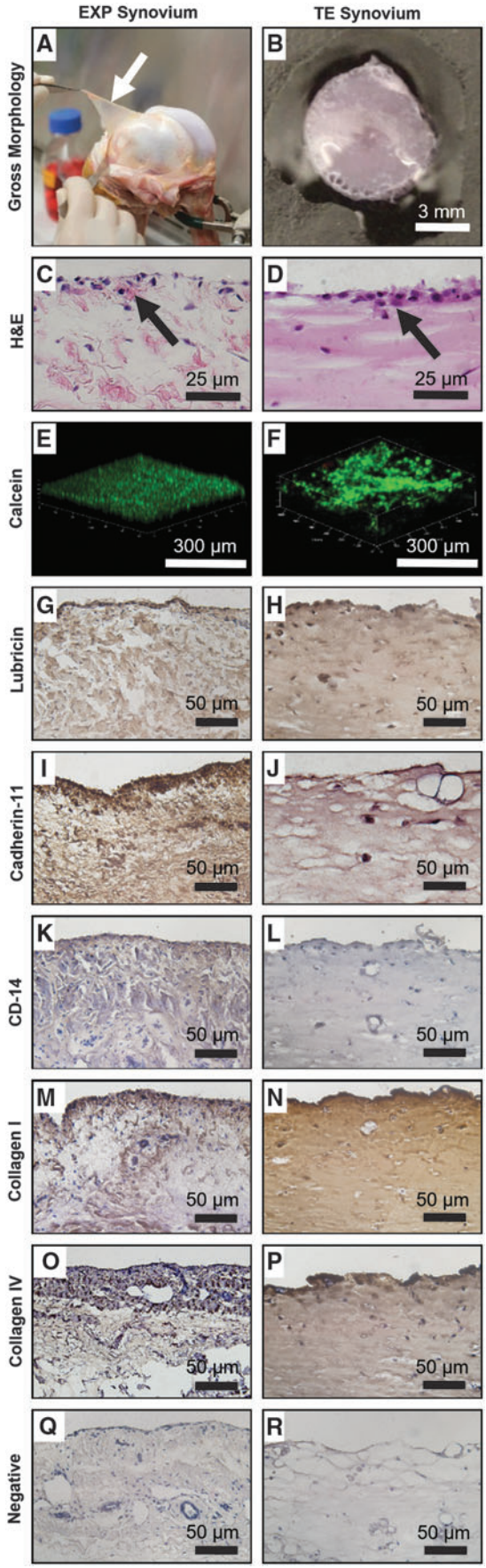

to the final DW of the associated specimens. NO values were normalized to the final DNA content of the specimens.

Agarose gel (0.5% w/v in TAE buffer) electrophoresis (~2.3 V/cm for 6 h) and subsequent staining with 0.005% Stains-All (Cat. No. E9379; Sigma) in 50% ethanol were used to determine relative HA molecular weight (MW) distributions for pooled TE and EXP samples.[47] A Hi-Mark™ prestained protein ladder (Cat. No. LC5699; ThermoFisher) and ~1.5–1.8 MDa HA (Cat. No. 53747; Sigma) were used as approximate MW standards. A solution of 50% (v/v) juvenile bovine synovial fluid in phosphate-buffered saline (PBS) was added as an additional comparison. ImageJ was used to generate size distribution histograms from imaged gels and quantify peak location and area under curve.

Histological and immunohistochemical characterization

Four percent paraformaldehyde-fixed samples (TE and EXP) were embedded in paraffin wax and sectioned in 8 μm slices. Deparaffinized sections were stained with hematoxylin and eosin (H&E) to determine cell distribution and with Picrosirius red to determine collagen distribution. Samples were immunohistochemically stained for collagen type I[5] (1:200, rabbit polyclonal, Cat. No. ab34710; Abcam), collagen type IV[5] (1:500, rabbit polyclonal, Cat. No. ab6586; Abcam), lubricin[29] (1:250, rabbit polyclonal, Cat. No. ab28484; Abcam), CD 14[48] (1:200, rabbit polyclonal, Cat. No. ab203294; Abcam), and cadherin-11[26] (1:40, goat polyclonal, Cat. No. AF1790; R&D Systems) using a 3,3′ Diaminobenzidine (DAB) Substrate Kit (Cat. No. ab64238; Abcam). Briefly, heat-mediated epitope retrieval was performed for 10 min at 98°C in citrate buffer (pH 6) before commencing the DAB protocol. The sections were counterstained with hematoxylin. Isotype controls were prepared to rule out nonspecific staining.

Functional assessment of tissue permeability

Three different solutions were prepared, each containing a different fluorescein isothiocyanate (FITC)-labeled dextran diluted in PBS (10 kDa, 0.5 mg/mL, Cat. No. D1820; 70 kDa, 0.5 mg/mL, Cat. No. D1822; and 500 kDa, 0.2 mg/

FIG. 3. Bovine EXP (*white arrow*) (day 0) and TE (mature, day 21) synovium exhibited similar structural characteristics **(A–F)** and protein expression **(G–R)**. Both tissues **(A, B)** displayed an opaque, flat, and membranous morphology. A 1–4 cell thick intimal lining layer (*black arrows*) was observed using H&E **(C, D)**; 3D z-stack reconstruction **(E, F)** with cells labeled with calcein-AM (*green*) showed similar cellular localization to the surface of the tissue with fewer subintimal cells. Positive immunohistochemical staining was visualized with 3,3′ diaminobenzidine Peroxidase and cells were counterstained with hematoxylin. Both tissues showed lubricin **(G, H)** and cadherin-11 expression **(I, J)**. CD14 expression was extremely low in EXP synovium **(K)**, as expected for ''healthy'' synovium containing primarily FLS, whereas TE synovium **(L)** had negative staining. Type I **(M, N)** and type IV **(O, P)** collagen, which are ECM components of the subintimal layer and intima, respectively, were also present in both tissues. Corresponding isotype controls **(Q, R)** showed the absence of nonspecific staining. 3D, three dimensional; H&E, hematoxylin and eosin; ECM, extracellular matrix.

mL, Cat. No. D7136; ThermoFisher). Small dextrans were selected to resemble the MW of the proinflammatory cytokines IL1α (17 kDa) and TNF-α (17 kDa), as well as TGFβ3 (27 kDa), matrix metalloproteinase (MMP)-2 (72 kDa), and small MW HA. Lubricin (200–400 kDa) concentrations are 0.3–0.4 mg/mL[22] and 0.11–0.18 mg/mL[22] in healthy and OA knees, respectively, whereas HA (27–10,000 kDa) concentrations are in the order of 1–4 mg/mL, depending on disease state.[22]

At time zero, 50 μL of FITC-labeled dextran in PBS solution was added to the upper (luminal) compartment of the Transwell ($N=7$–8 per medium-solute size pairing) (Fig. 2C). PBS (150 μL) was added below the Transwell (basolateral) and was collected and replenished with fresh PBS at 0-, 1-, 2-, 4-, 8-, 24-, 48-, and 72-h time points. The basolateral solute concentration was quantified for each time point using a fluorescent plate reader (SpectraFluor Plus; Tecan) at an excitation and emission wavelength of 495 and 519 nm, respectively.

Clearance, defined as the amount of dextran collected from the basolateral compartment as a function of the starting amount of dextran in the luminal compartment, was plotted as a function of time. Apparent permeability (P_d) was computed as a function of solute flux (J_s), area of the filter (S), and solute concentration difference in the luminal and basolateral compartment (ΔC): $P_d = J_s/(S\Delta C)$.[49,50] For this computation, it was assumed that solute flux was determined entirely by diffusion.

In a similar manner, permeability of 70 kDa dextran was assessed in CTL- and IL-treated bovine EXPs ($N=3$–4) by affixing a piece of tissue to a larger 6.5 mm Transwell using a silicone gasket (Fig. 2B, D). The DEX group was omitted from EXP transport analysis due to sample size limitations related to the large amount of EXP tissue required to make these measurements. Solute transport in native EXPs was visualized qualitatively using confocal imaging.

Synovial macrophage isolation and expansion

Synovial EXP tissue from juvenile bovine ($n=2$–4) or human OA ($n=3$) knees was digested in collagenase type II for 2 h at 37°C. Isolated cells were counted using a hemocytometer before and after performing a CD14 Dynabeads™ (Cat. No. 11149D; ThermoFisher) negative selection protocol. Briefly, the mixed cell population of synovial cells was incubated in Dynabeads and magnetically separated based on CD14 expression. For passaging, viable MLS ($CD14^+$) were plated at a density of 1.76×10^3 cells/cm^2 and expanded for two passages in αMEM containing 10% FBS, 1% antibiotic–antimycotic, and 10 ng/ml macrophage colony-stimulating factor (Cat. No. PHC9504; ThermoFisher).[51]

For quantification of $CD14^+$ (MLS) and $CD14^-$ (FLS) cells in EXP tissues, parallel groups were counted with Dynabeads (to determine relative ratio) and quantified using the Picogreen DNA assay (to determine total cell content per DW). The resulting ratio and total cell number were combined to give an approximation of overall cell phenotype.

Macrophage-like synoviocyte co-culture and tracking

Passage 2 bovine MLS were prelabeled using DiI lipophilic membrane dye (Cat. No. V22885; ThermoFisher), while passage 2 bovine FLS remained unlabeled. TE constructs were created as previously described with three different FLS to MLS ratios: 100% FLS, 50% FLS +50% MLS, or 100% MLS. Each group had an initial cell concentration of 5×10^6 cells/mL.

Preculture followed by CTL or IL culture conditions ($N=2$), as described earlier, was conducted and specimens were processed for immunofluorescence. Briefly, sections were deparaffinized and heat-mediated epitope retrieval was performed for 10 min at 98°C in citrate buffer (pH 6). Sections were incubated overnight in CD14 primary antibody (1:200, rabbit polyclonal, Cat. No. ab203294; Abcam) followed by a 1-h incubation in Alexa Fluor 488 secondary antibody (1:200, goat anti-rabbit, Cat. No. ab150077; Abcam). The sections were counterstained with 4′,6-diamidino-2-phenylindole.

Statistical analysis

Data sets were tested for normality and homogeneity using the Kolmogorov-Smirnov Test and Bartlett's test, respectively. If possible, nonnormal data were log-transformed to achieve normal distribution for subsequent parametric tests. Otherwise, nonnormal and nonhomogeneous bovine data were analyzed using the Kruskal Wallis test and Dunn's *post-hoc* test. Non-normal and nonhomogeneous human data were analyzed using the paired Friedman test and Dunn's *post-hoc* test. Normal and homogeneous data sets were analyzed using one- or two-way analysis of variance with Tukey *post-hoc* test. A Pearson (*r*) or Spearman (rs) correlation coefficient was computed for relevant comparisons with $\alpha=0.05$. All statistical tests were performed in GraphPad Prism 7 (La Jolla, CA). Values are presented as mean ± standard deviation.

Results

Study 1. Baseline comparison of synovium-specific structure and composition

Mature day 21 TE synovium exhibited structural characteristics of native synovium. TE synovium had an opaque, flat morphology, reminiscent of the membranous appearance of native tissue EXPs (Fig. 3A, B). The formation of the intimal lining, a key characteristic of synovium, was confirmed with H&E (Fig. 3C, D). Three-dimensional z-stack reconstructions of confocal images showed similar patterns of cellular organization in each tissue (Fig. 3E, F). In addition, TE synovium expressed critical proteins of interest in the native synovium. Lubricin (Fig. 3G, H), cadherin-11 (Fig. 3I, J), collagen type I (Fig. 3M, N), and collagen type IV (Fig. 3O, P) were highly expressed in the intimal lining layer, and throughout the subintima. CD14 expression (Fig. 3K, L), indicative of MLS or monocyte phenotype, was low in each tissue.

Study 2a. Comparison of biological response to proinflammatory cytokine or corticosteroid

Robust lubricin staining was observed in EXP and TE synovium for both CTL and IL groups, with comparatively weaker staining in DEX groups (Fig. 4A). Gel electrophoresis of pooled specimens (Fig. 4B, C) showed that both CTL- and DEX-treated EXP and TE specimens had greater proportions of high MW HA compared to their IL-treated counterparts. The 1.5 MDa HA standard and bovine synovial fluid contained predominantly high (>460 kDa) MW HA, although a large size range with multiple peaks was observed in each (Fig. 4D).

Furthermore, of the high MW HA (>460 kDa) in EXP specimens, CTL- and DEX-treated EXPs had predominantly

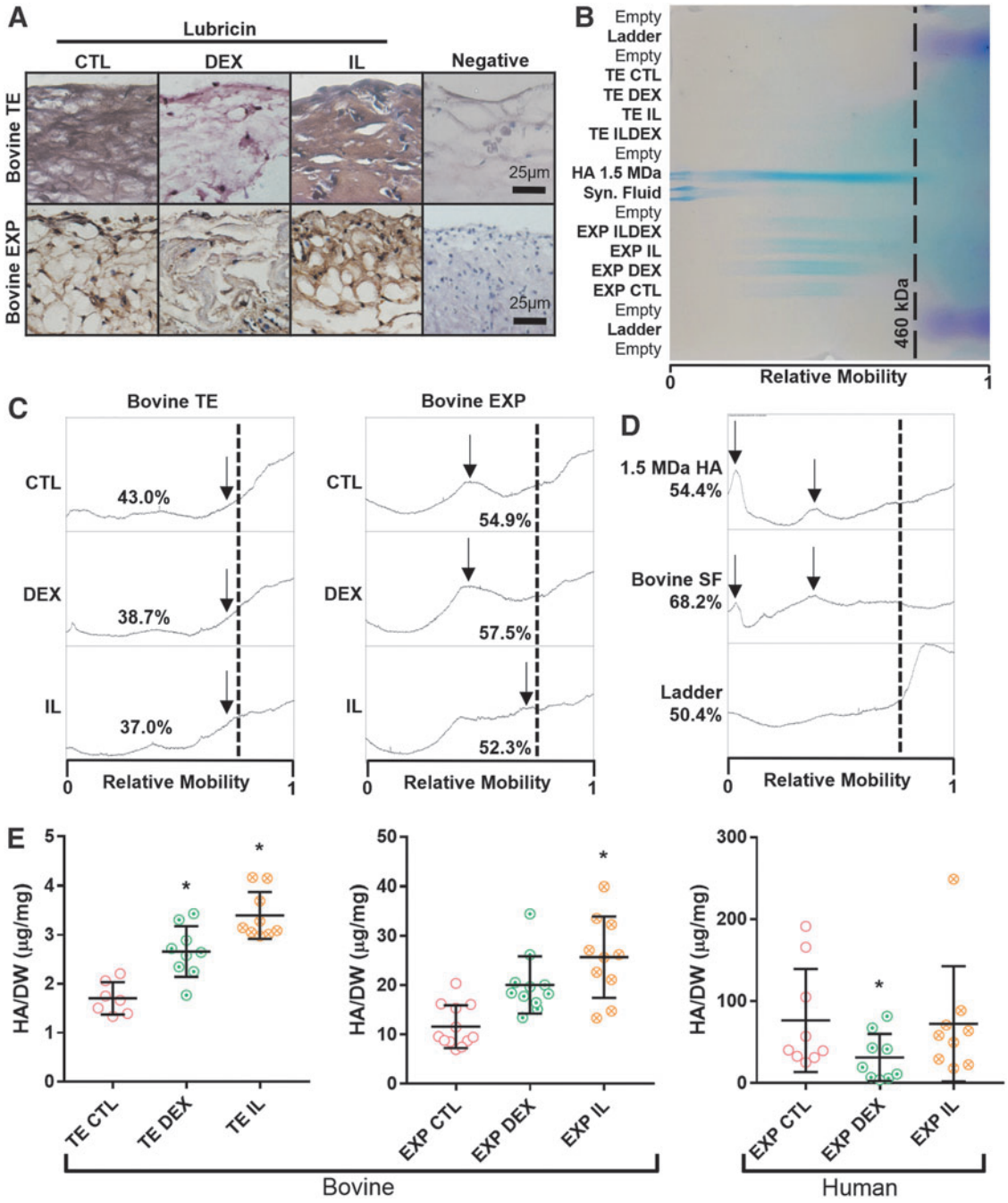

FIG. 4. **(A)** Robust lubricin expression (*reddish brown*) was observed in CTL and IL groups for both EXP and TE synovium, with comparatively weaker staining in DEX groups. **(B)** Agarose gel electrophoresis (HA, *blue*; ladder, *purple*) showed approximate HA size distribution of **(C)** pooled experimental groups and **(D)** standard molecules. **(C)** In both EXP and TE synovium, wide HA MW distributions were observed, with the highest proportion of high MW HA (lower relative mobility) being estimated in CTL- and DEX-treated groups. Peaks (*arrows*) represented mobility of the predominant high MW HA for a given group. **(D)** The upper size limit of the ladder was 460 kDa (*dotted line*), which was used as a cutoff point to approximate the relative amounts of small and large MW HA in the given sample. Lower MWs could not be accurately resolved in the given gel conditions (low agarose concentration and high voltage) that were otherwise necessary for HA mobility. **(E)** Overall, bovine TE and EXP synovium had elevated HA secretion in response to DEX and IL treatment. In human EXP synovium, HA secretion was depressed by DEX and unaltered by IL treatment, $*p < 0.05$ versus CTL. HA, hyaluronic acid; MW, molecular weight; IL, interleukin; DEX, dexamethasone.

higher MW HA than IL-treated EXPs. HA secretion in IL groups was significantly higher than CTL in TE synovium and bovine EXPs ($p<0.05$) with a near twofold increase, and to a lesser extent in TE synovium treated with DEX ($p<0.05$) (Fig. 4E). Human OA EXPs treated with DEX had significantly lower HA secretion compared to CTL ($p<0.05$), while IL-treated EXPs did not differ significantly from CTL.

Study 2b. Structural and transport changes in response to proinflammatory cytokine or corticosteroid

Total collagen content, normalized to average initial collagen content in the given tissue type, was significantly lower in DEX-treated TE synovium compared to CTL ($p<0.05$) (Fig. 5A). A similar trend was observed in IL-treated TE synovium ($p=0.2698$). No significant differences were observed in collagen of bovine or human OA EXPs (Fig. 5B, C). DNA content, normalized to initial DNA content, was elevated in IL-treated TE ($p=0.1631$) and bovine EXP ($p=0.1357$) synovium relative to their CTL counterparts, whereas no significant difference was observed in human OA EXPs (Fig. 5D–F). Combining the two measures, the relative change in ratio of collagen to DNA (COL/DNA) was significantly lower in TE DEX and TE IL relative to TE CTL ($p<0.05$) (Fig. 5G). Similarly, a trend of decreased COL/DNA was observed in bovine EXP IL compared to CTL ($p=0.1035$) (Fig. 5H). Large variation in DNA content of human EXP specimens limited statistical analyses.

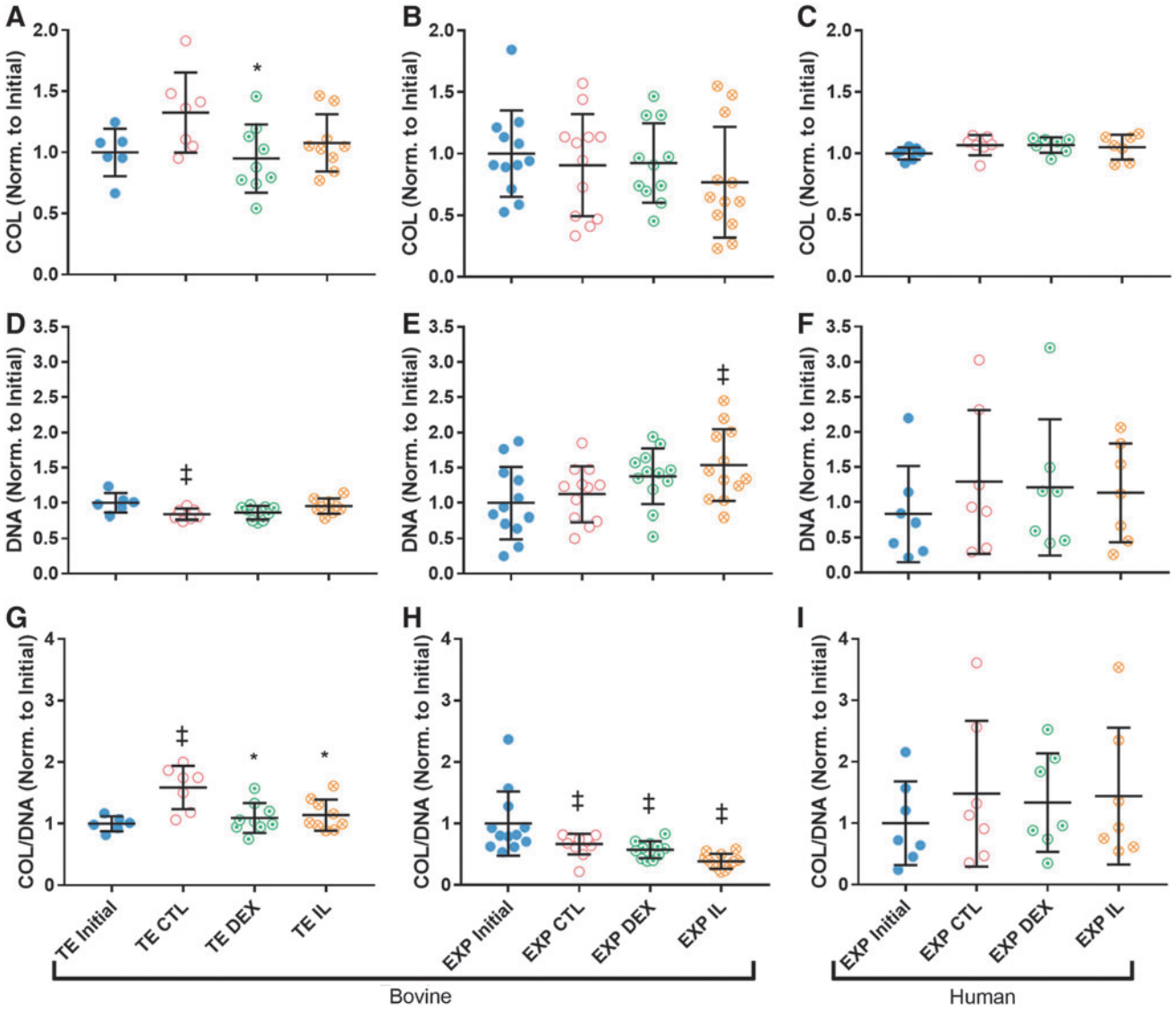

FIG. 5. **(A)** Change in total collagen was significantly lower in DEX-treated TE synovium relative to CTL ($p<0.05$), and a similar trend was observed in IL-treated TE synovium ($p=0.2698$). Total collagen was statistically unchanged in all **(B)** bovine and **(C)** human EXP groups. Change in DNA was elevated with IL treatment relative to CTL for **(D)** bovine TE synovium ($p=0.1631$) and **(E)** EXP synovium ($p=0.1357$). DNA significantly decreased compared to initial values in TE CTL and increased compared to initial values in EXP IL ($p<0.05$). DNA was unchanged in **(F)** human EXP groups. Change in COL/DNA was significantly lower in DEX- and IL-treated groups compared to CTL for **(G)** bovine TE synovium ($p<0.05$), and similar trends were seen for **(H)** EXP IL ($p=0.1035$). COL/DNA was unchanged in **(I)** human EXP groups. $^{*}p<0.05$ versus CTL, $^{‡}p<0.05$ versus Initial. COL, collagen.

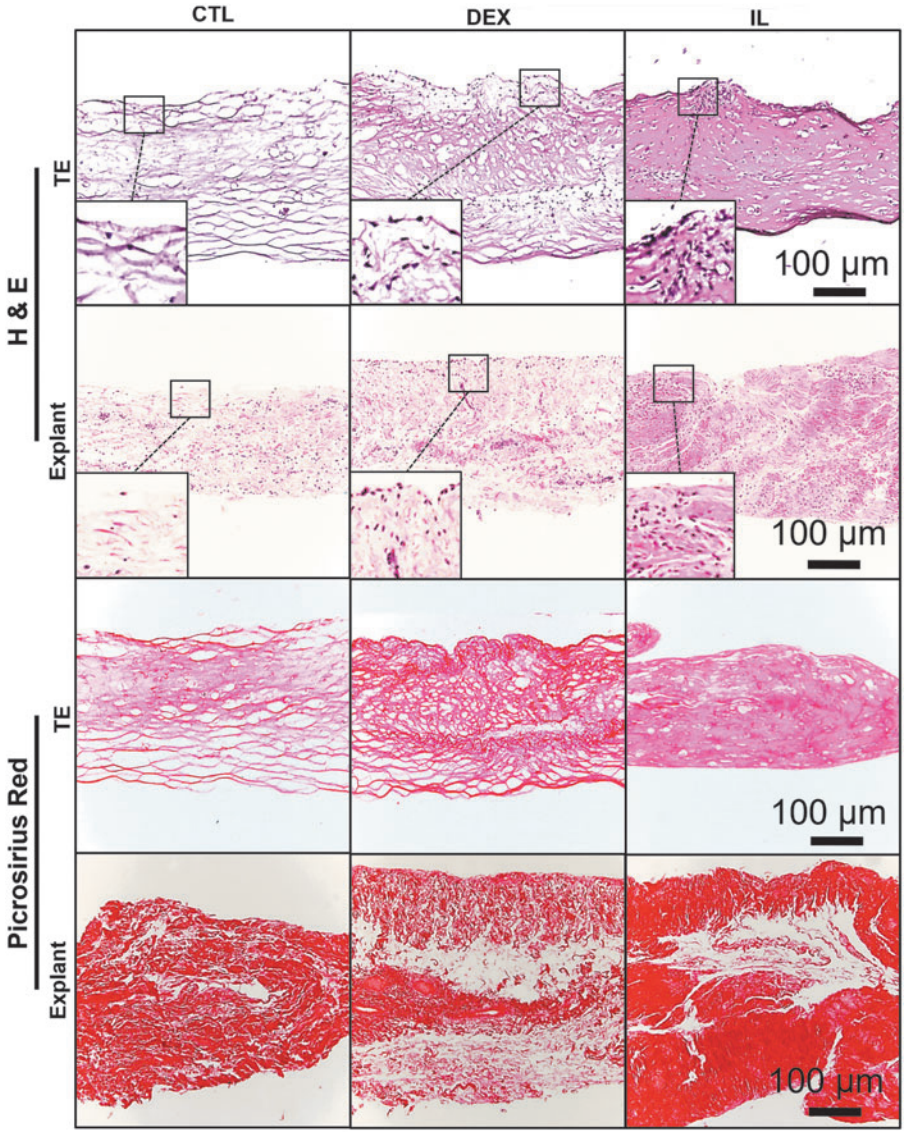

FIG. 6. Similarities were observed in structural changes undergone by TE and EXP synovium, as visualized with H&E and Picrosirius red staining. CTL specimens were especially fibrous, with strong Picrosirius red staining and associated large gaps present in the ECM. DEX specimens had increased intimal cellularity and slightly denser matrix staining. IL specimens had further increased intimal cellularity and very dense collagen matrix present throughout the tissue.

Similar structural changes were observed in TE and EXP synovium, as visualized with H&E and Picrosirius red histology (Fig. 6). CTL specimens were especially fibrous, with strong Picrosirius red staining and associated large gaps present in the ECM. DEX specimens had increased intimal cellularity and slightly denser matrix. IL specimens had further increased intimal cellularity and very dense collagen matrix present throughout the tissue.

For solute transport analysis (Fig. 7), the two separate fluid reservoirs modeled different compartments within the joint. The luminal compartment modeled synovial fluid, while the basolateral compartment modeled the extracapsular space. Total clearance over 72 h (Fig. 7A, C, and E) mimicked differences in permeability (Fig. 7B, D, and F) in each group, with higher clearance correlating to higher permeability values, as expected. Cell-free Matrigel controls (not plotted) consistently had significantly higher clearance than TE constructs over the 72-h measurement period ($p<0.05$). Cell-free controls versus TE constructs had 72-h dextran clearances of ($\sim$56% vs. $\sim$25%) for 10 kDa, ($\sim$24% vs. $\sim$13%) for 70 kDa, and ($\sim$17% vs. $\sim$5%) for 500 kDa.

Overall, permeability in TE synovium (Fig. 7A–F) was significantly lower with increasing solute MW ($p<0.05$). Both DEX and IL resulted in decreased permeability of the 70 kDa solute ($p<0.05$), with approximate decreases of 28% and 26%, respectively (Fig. 7D). In TE synovium, decreased collagen to DNA ratio (COL/DNA) was strongly correlated with observed decreases in permeability of 70 kDa dextran [$r(2)=0.9736$, $p=0.0264$]. Specifically, DEX and IL specimens had lower COL/DNA compared to CTL (Fig. 5G), and similarly had lower permeability (Fig. 7D). No significant differences or correlations were observed with the 10 and 500 kDa solutes.

Total 72-h clearance of 70 kDa dextran was significantly higher in EXP compared to TE specimens ($p<0.05$); however, variance was quite high compared to TE constructs. Permeability of 70 kDa dextran was statistically similar in

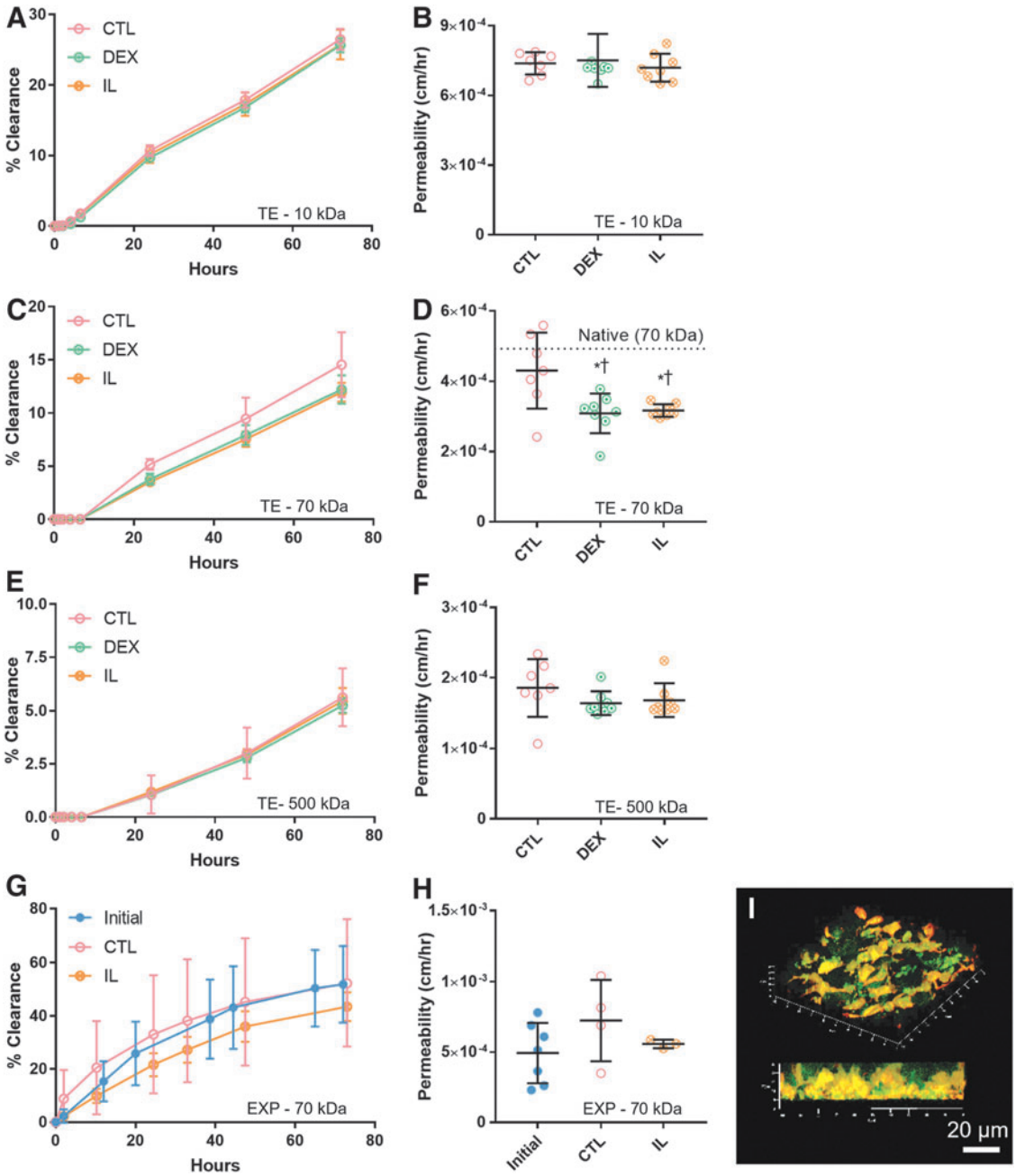

FIG. 7. Cumulative clearance of dextran over time and corresponding permeability values were presented for 10, 70, and 500 kDa sizes in TE specimens **(A–F)** and for the 70 kDa size in bovine EXP specimens **(G, H)**. **(D)** Both DEX- and IL-treated TE groups exhibited decreased permeability relative to CTL with 70 kDa dextran only. Permeability of 70 kDa dextran in CTL did not differ significantly from native tissue [*dotted line*, value from **(H)**], whereas DEX and IL specimens were significantly lower (*$p<0.05$ vs. CTL, $^{\dagger}p<0.05$ vs. native). **(G, H)** In EXP synovium ($N=3$–4), permeability in CTL increased over time and was higher than IL-treated tissue, but neither observation was statistically significant ($p=0.0941$ and $p=0.3448$, respectively). **(I)** Representative 3D confocal image of 70 kDa FITC-Dextran (*green*) and resident cells (*red-orange*) within a living synovium EXP showed diffusion occurring in intercellular spaces.

TE synovium and bovine EXPs, with coefficients of $4.3\times10^{-4}\pm1.1\times10^{-4}$ cm/h and $4.9\times10^{-4}\pm2.1\times10^{-4}$ cm/h, respectively. Permeability of 70 kDa dextran in CTL bovine EXPs increased twofold ($p=0.0941$), while IL-treated EXPs remained unchanged ($p=0.88$) (Fig. 7H). No significant correlation between permeability coefficient and COL/DNA was observed in bovine EXPs [rs(1) = –0.3210, $p=0.7920$]. However, confocal imaging showed diffusion primarily occurring in the intercellular spaces (Fig. 7I).

Study 3a. Synovial inflammation and correlation to CD14 expression

NO production per DNA (NO/DNA) was elevated in IL-treated TE synovium, bovine EXPs, and human OA EXPs compared to corresponding DEX groups ($p<0.05$) (Fig. 8A).

Day 0 bovine EXPs consisted primarily (>90%) of $CD14^{-}$ cells (Fig. 8C), which was consistent with CD14 immunostaining (reddish brown) (Fig. 8B). This ratio of

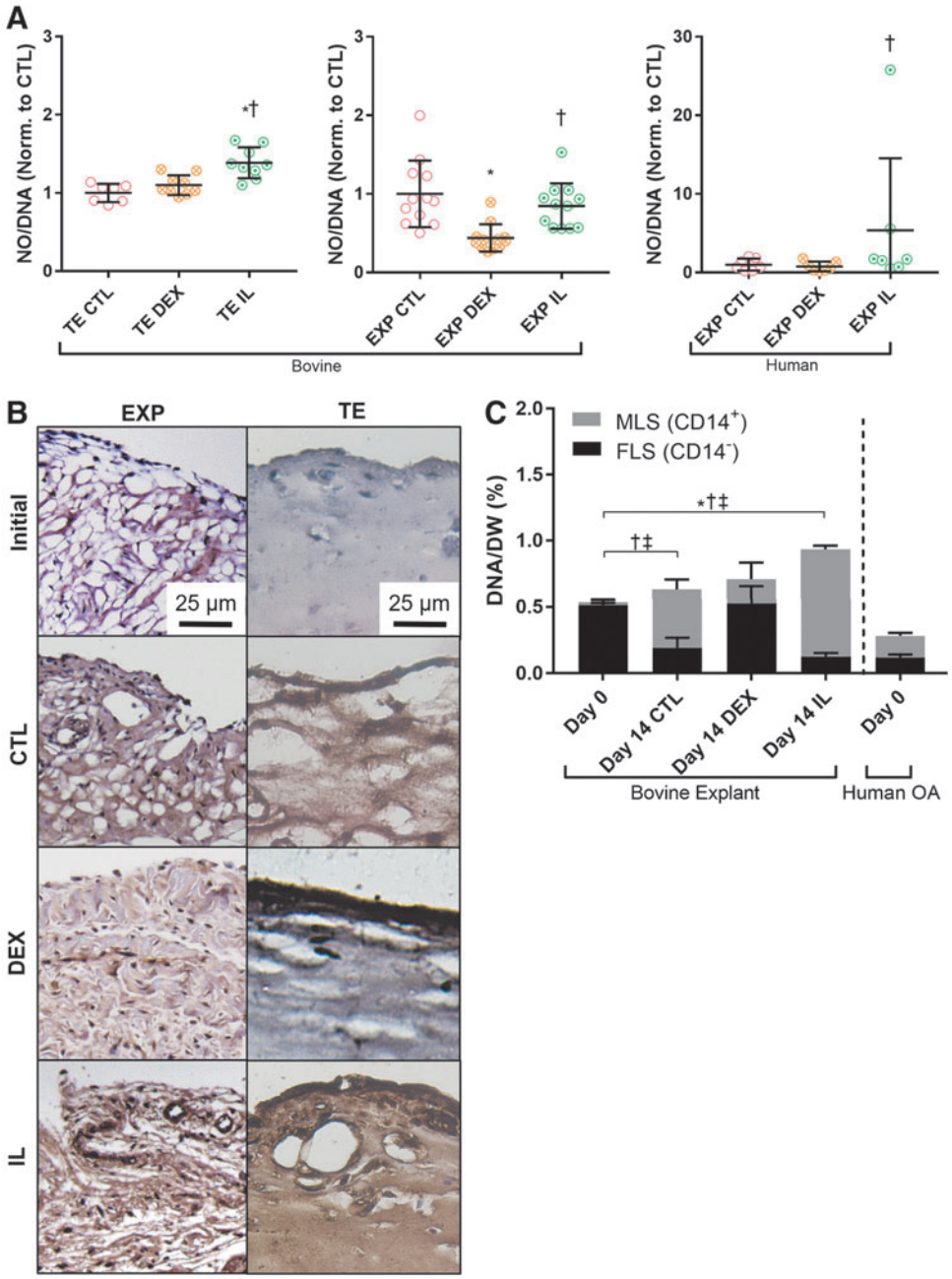

FIG. 8. **(A)** Bovine TE and EXP synovium, as well as human OA EXPs, showed elevated nitric oxide production in response to IL treatment, $*p<0.05$ versus CTL, $^{\dagger}p<0.05$ versus DEX. **(B)** Elevated CD14 expression (*reddish brown*) was observed in both TE and EXP tissue treated with IL. An increase was also seen in CTL groups, but CD14 staining was less intense for DEX specimens in both tissue types. **(C)** The phenotype ratio of MLS ($CD14^+$) to FLS ($CD14^-$) in EXP tissue was maintained by DEX. In CTL- and IL-treated tissue, MLS content increased and FLS content decreased. Total cell content increased with IL treatment; $*p<0.05$ (total DNA), $^{\dagger}p<0.05$ (FLS), $^{\ddagger}p<0.05$ (MLS).

$CD14^+$ to $CD14^-$ was maintained over 14 days with DEX ($p<0.05$) (Fig. 8C). In CTL- and IL-treated EXPs, both $CD14^+$ and overall cell content (% DNA/DW) increased significantly ($p<0.05$). Concurrently, $CD14^-$ content decreased significantly in both groups, dropping to $\sim$30% and 13% of total cells, respectively. Day 0 human OA EXPs contained lower DNA/DW than bovine EXP specimens; however, $CD14^+$ constituted over 50% of the total cell population in OA EXPs.

Study 3b. FLS versus MLS role in structural reorganization

The DiI membrane dye (red) robustly labeled MLS, and initial FLS to MLS ratios were qualitatively maintained over 14 days in CTL culture (Fig. 9A). Furthermore, the CD14 phenotype appeared to be stable, with red-labeled MLS also exhibiting strong positive expression of CD14 (green), while nonlabeled FLS did not express CD14.

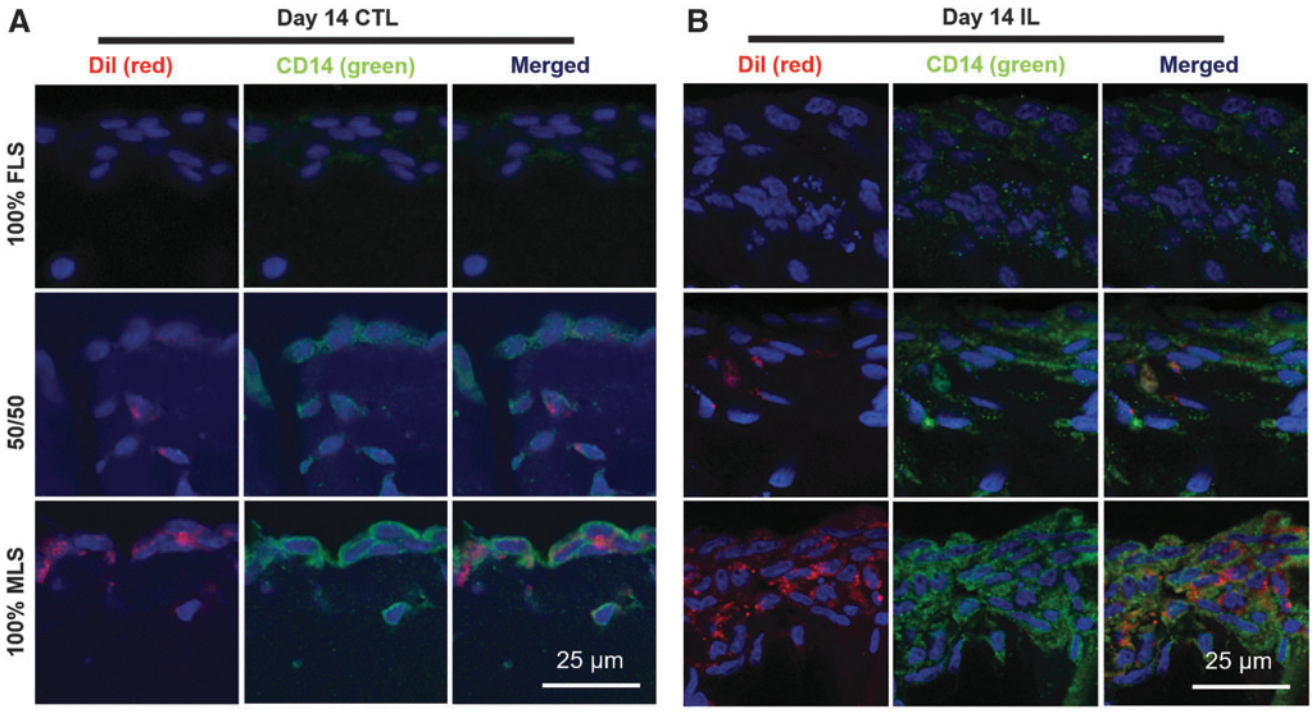

FIG. 9. TE synovium with prelabeled MLS (DiI, *red*) and varying ratios of unlabeled FLS was cultured for 2 weeks in CTL- or IL-supplemented media and all cells subsequently counterstained with 4′,6-diamidino-2-phenylindole (*blue*). In both **(A)** CTL and **(B)** IL groups, DiI (*red*) was co-localized with intense CD-14 expression (*green*). Intimal lining formation was apparent in all groups **(A, B)**, regardless of cell type, with intimal hyperplasia apparent in groups treated with IL **(B)**.

Intimal layer formation was visible in all groups (Fig. 9A, B). When treated with IL, the degree of intimal hyperplasia appeared to be dependent on the initial cell ratio, with higher MLS to FLS ratios resulting in a thicker intima (Fig. 9B).

Discussion

The findings of this work support the hypothesis that a sheet-like, stratified FLS-Matrigel-based engineered synovium tissue can be formed to mimic both chemical-induced structural and compositional changes observed in native tissues. Furthermore, these changes can be related to altered solute permeability. Similarities in structural, biochemical, and solute transport function were observed in bovine TE synovium and native synovium EXPs, in the presence of proinflammatory cytokine or corticosteroid.

It is anticipated that our engineered synovium, with the intrinsic benefits associated with well-controlled *in vitro* models and the potential for reverse engineering native tissue, will provide new insights to the underlying structure–function relationships of this specialized connective tissue. This versatile biofidelic culture model can serve as a test bed to explore the biological role of the synovium in healthy joint homeostasis as well as the efficacy of new treatments targeting the synovium's role in the pathology of joint diseases such as OA.[52,53]

The FLS-only TE synovium in Study 1 and 2 exhibited a defined intimal lining layer and expressed lubricin and cadherin-11, among other markers of native synovium (Fig. 3). HA secretion was increased in response to IL and DEX, and this same trend was observed for native EXPs (Fig. 4E). Additionally, relative size determination by gel electrophoresis showed a shift to lower MW HA in IL-treated specimens compared to CTL and DEX (Fig. 4B, C).

A similar trend has been observed in OA patients, where the proportion of proinflammatory, low MW HA in the joint[54] tends to increase due to the breakdown of larger MW HA.[55] This shift in HA size is likely in response to increased concentrations of proinflammatory mediators such as MMPs, NO, and PGE2, which have been observed in healthy and OA EXPs exposed to cytokine insult.[52,53,56–59] On the other hand, corticosteroids are known to have a significant anti-inflammatory effect and to modulate cell biosynthesis in the joint,[39] presumably counteracting HA breakdown.[60] In fact, IL increased and DEX decreased NO production in our specimens, as expected (Fig. 8A).

The concentration of lubricin, another lubricant molecule, was decreased in the ECM of DEX-treated and CTL bovine EXPs (Fig. 4A). It is possible that greater levels of secreted lubricants in the media (ie. HA) for DEX groups are correlated to lower levels of lubricin within the tissue itself; however, additional studies will be required to confirm this.

It is known that OA synovial fluid contains decreased concentrations of lubricin, [refs] which is seemingly at odds with reports that OA FLS rapidly proliferate and secrete more lubricant molecules (e.g., HA and lubricin) when treated with IL-1β and TNF-α *in vitro*.[1,2,63–66] Overall, it is presumed that the relative balance between aberrant cytokine/lubricant production and altered transport properties, along with degree of joint effusion, determines solute concentration in the synovial fluid.

Permeability of 500 kDa dextran was $\sim 1.6–1.9 \times 10^{-4}$ cm/h in TE synovium, which is similar to that of lubricin and HA ($\sim 0.36–1.8 \times 10^{-4}$ cm/h) in membranes of physiologic pore size (50 nm).[67] Permeability of 70 kDa dextran was statistically similar in TE synovium and bovine EXPs, with coefficients of $4.3 \times 10^{-4} \pm 1.1 \times 10^{-4}$ cm/h and $4.9 \times 10^{-4} \pm 2.1 \times 10^{-4}$ cm/h, respectively. Furthermore, the observed relationship between increasing solute size and decreased permeability parallels *in vivo* findings of the rabbit knee, which showed increased clearance of low MW HA (≤500 kDa) compared to high MW HA (~ 2200 kDa).[68,69]

As 10 kDa dextran permeability was similar across studies, this size solute can likely diffuse freely through even small intercellular spaces. On the other hand, molecules of 500 kDa and above diffuse very slowly. Future studies can investigate whether more accurate modeling, including computational analyses of the transport, can resolve differences in behavior of higher MW solutes.

Under the conditions of these studies, treating TE synovium with DEX or IL resulted in an $\sim 20\%$ reduction in 70 kDa dextran permeability (Fig. 7D). A similar decrease in permeability was observed in IL versus CTL bovine EXP tissues; however, there was a high degree of statistical variance arising from the inherent challenges in harvesting uniform synovium samples from the joint (Fig. 7H).

This functional change was related to lower collagen in DEX-treated TE synovium and greater DNA in TE synovium treated with IL. In fact, the relative ratio of COL/DNA (i.e., ECM vs. cells) in DEX- and IL-treated groups for both TE synovium and bovine EXPs was lower than CTL (Fig. 5G, H). In TE synovium, this lower COL/DNA was strongly correlated with observed lower permeability of 70 kDa dextran ($r^2 = 0.9736$, $p = 0.0264$). No significant correlation was detected in bovine EXPs, so it is unclear to what extent the ECM contributes to native tissue transport behavior.

Others have described similar solute behavior in the synovium, which is facilitated by ECM volume fractions (primarily collagen fibrils and glycosaminoglycans) and limited by the space occupied by cells.[67] The observations in this study support this mechanism; solute diffusion was visible solely in the interstitial matrix (Fig. 7I). This potential mechanism is further supported by histological findings (Fig. 6), which showed intimal hyperplasia in both DEX- and IL-treated TE specimens. This structural change was mirrored in explanted tissue, and increased collagen compaction in IL-treated groups relative to CTL was observed as well. Future studies will be necessary to assess the relative importance of these structural changes to transport function compared to bulk ECM content and inflammatory characteristics.

Despite the similarities in transport characteristics of native and engineered synovium presented herein, it should be noted that our *in vitro* solute transport results are seemingly in contrast with reports of increased HA clearance from arthritic joints,[70,71] as well as elevated degradative enzymes associated with tissue breakdown and possible increased permeability.[72] Aside from the increased complexity of interpreting solute transport from the native synovial joint, it is speculated that this difference may be due to competing factors. While breakdown of HA may lead to higher clearance, the thickening of the intimal layer may hinder transport.

The downward shift in HA MW was recreated in our EXP and TE synovium experiments in response to IL (Fig. 4B, C). A recent study of dextran clearance in destabilized rat knees supports this hypothesis as well, showing slower transport of 500 kDa dextran and an apparent thickening of synovium in the destabilized joints.[73]

While the results are promising, it is possible that dextran does not fully recreate the complex tertiary structure of large MW HA or exhibit the same binding characteristics. Future work should examine various sizes of HA; however, endogenous HA synthesis/breakdown in cultures and the high polydispersity of commercially available HA products may confound results. Furthermore, as additional variables are added to increase the complexity of our TE model, such as to examine the effects of vascular-mediated clearance,[18,22] synovial fluid shear, hydrostatic pressure, and strain-dependent permeability, there may be more convergence of our culture findings with those *in vivo*.

While correlations between structure and function may be limited by the different size Transwells used, it was necessary to fabricate engineered synovium of dimensions better suited for a particular target measurement. The larger 6.5 mm Transwell system was used to grow specimens that produced measurable levels of matrix and lubricants. A scaled-down 4.26 mm system was adopted to enable the larger sample sizes required to resolve changes in transport. Importantly, comparisons between TE constructs subjected to different treatments were performed on engineered synovium derived from the same size Transwell.

While it is possible that tissue properties may be somewhat dependent on the Transwell size, similar structural and chemical changes were observed in response to proinflammatory cytokines to those reported for other configurations, such as engineered synovial microtissues[36] and FLS monolayers.[2] For comparisons of TE synovium, initial construct dimensions as well as cell and Matrigel concentrations were kept consistent. Nevertheless, future studies will incorporate additional ELISAs and sensitive measurement techniques to allow all measurements in the scaled-down, high-throughput version of the system.

Human OA EXPs were predominantly composed of $CD14^+$ cells and had significantly decreased HA secretion when treated with DEX, one of the few cases where human OA EXP behavior diverged from the TE model (Fig. 4E). In healthy synovium, MLS make up <10% of the cell content. The hyperplastic synovium response includes a drastically changing distribution and quantity of FLS and MLS depending on OA stage.[74,75]

It is likely that a significant portion of $CD14^+$ cells in the OA human tissue were blood-derived cells, rather than resident MLS.[18] This may partially explain why human OA cells were far more responsive to IL than bovine cells in secreting NO, a proinflammatory mediator (Fig. 8A). Infiltration of macrophages and activated fibroblasts into the joint is a hallmark of RA, and it is unknown to what degree this is seen in OA synovium.

Interestingly, an apparent phenotypic shift was seen in our bovine EXP cultures (Fig. 8B, C) and may help to explain the similarity in the biological response of the FLS-based TE synovium and native tissues (Study 2). CTL- and IL-treated bovine EXPs had an increase in $CD14^+$ cells and decrease in $CD14^-$ cells, whereas treatment with DEX maintained CD14

expression levels. There is precedent for human fibroblasts to express and secrete soluble CD14[76] and other markers of M1-activated macrophages[77] when exposed to an inflammatory environment, so it is possible that the phenotypic shift was partially due to transdifferentiation of FLS.[78,79]

It is anticipated that the ability to define initial FLS to MLS ratios of the TE synovium may be important for modeling different stages of disease as well as understanding interactions between these cell types (Study 3), which is not possible *in vivo* or with native synovium EXPs (Fig. 9). The hyperplastic response to IL seemed to be exacerbated by the presence of MLS (Fig. 9B), which may have significant implications for transport as well. In future studies, efforts can be expanded to include other cell types important in OA, such as blood-derived monocytes and lymphocytes. Furthermore, it will be informative to observe relative M1/M2 phenotype of resident and nonresident immune cells and correlating this to NO or PGE2 concentration.

The FLS-based TE synovium described herein was shown to recapitulate the gross morphological and biological responses (e.g., NO and HA synthesis) of native synovium to applied IL and DEX (Study 1). Importantly, IL-treated engineered and native bovine synovium displayed characteristics of human OA synovium. This relatively simple yet biomimetic synovium model will allow robust investigation of cellular mechanisms and macroscale tissue behavior in a controlled and repeatable system (e.g., Study 2). With the ability to add increasing degrees of complexity (e.g., Study 3), this model allows investigation of the role that synovial cells and their ECM play in the regulatory transport function of the synovium in diarthrodial joint health and disease. It is anticipated that a better understanding of synovium transport would support efforts to characterize, design, and modify biological compounds and pharmaceutical agents that may be more effective at restoring joint health.

Acknowledgments

This work was supported by R01AR068133, R01AR 069668, T32AR059028, and Orthopedic Scientific Research Foundation.

Disclosure Statement

No competing financial interests exist.

References

1. Blewis, M.E., Lao, B.J., Jadin, K.D., *et al*. Semi-permeable membrane retention of synovial fluid lubricants hyaluronan and proteoglycan 4 for a biomimetic bioreactor. Biotechnol Bioeng **106,** 149, 2010.
2. Blewis, M.E., Lao, B.J., Schumacher, B.L., Bugbee, W.D., Sah, R.L., and Firestein, G.S. Interactive cytokine regulation of synoviocyte lubricant secretion. Tissue Eng Part A **16,** 1329, 2010.
3. Schmidt, T.A., and Sah, R.L. Effect of synovial fluid on boundary lubrication of articular cartilage. Osteoarthritis Cartilage **15,** 35, 2007.
4. Kiener, H.P., Watts, G.F.M., Cui, Y., *et al*. Synovial fibroblasts self-direct multicellular lining architecture and synthetic function in three-dimensional organ culture. Arthritis Rheum **62,** 742, 2010.
5. Smith, M.D. The normal synovium. Open Rheumatol J **5,** 100, 2011.
6. Barland, P., Novikoff, A.B., and Hamerman, D. Electron microscopy of the human synovial membrane. J Cell Biol **14,** 207, 1962.
7. Valencia, X., Higgins, J.M.G., Kiener, H.P., *et al*. Cadherin-11 provides specific cellular adhesion between fibroblast-like synoviocytes. J Exp Med **200,** 1673, 2004.
8. Pelletier, J.P., Martel-Pelletier, J., and Abramson, S.B. Osteoarthritis, an inflammatory disease: potential implication for the selection of new therapeutic targets. Arthritis Rheum **44,** 1237, 2001.
9. Shibakawa, A., Aoki, H., Masuko-Hongo, K., *et al*. Presence of pannus-like tissue on osteoarthritic cartilage and its histological character. Osteoarthritis Cartilage **11,** 133, 2003.
10. Yuan, G.-H., Tanaka, V.M.D.M., Masuko-Hongo, K., *et al*. Characterization of cells from pannus-like tissue over articular cartilage of advanced osteoarthritis. Osteoarthritis Cartilage **12,** 38, 2004.
11. Mathiessen, A., and Conaghan, P.G. Synovitis in osteoarthritis: current understanding with therapeutic implications. Arthritis Res Ther **19,** 18, 2017.
12. Wenham, C.Y.J., and Conaghan, P.G. The role of synovitis in osteoarthritis. Ther Adv Musculoskelet Dis **2,** 349, 2010.
13. Scanzello, C.R., and Goldring, S.R. The role of synovitis in osteoarthritis pathogenesis. Bone **51,** 249, 2012.
14. Kiener, H.P., Lee, D.M., Agarwal, S.K., and Brenner, M.B. Cadherin-11 induces rheumatoid arthritis fibroblast-like synoviocytes to form lining layers in vitro. Am J Pathol **168,** 1486, 2006.
15. Smith, M.D., Triantafillou, S., Parker, A., Youssef, P.P., and Coleman, M. Synovial membrane inflammation and cytokine production in patients with early osteoarthritis. J Rheumatol **24,** 365, 1997.
16. Sutton, S., Clutterbuck, A., Harris, P., *et al*. The contribution of the synovium, synovial derived inflammatory cytokines and neuropeptides to the pathogenesis of osteoarthritis. Vet J **179,** 10, 2009.
17. Hügle, T., and Geurts, J. What drives osteoarthritis? Synovial versus subchondral bone pathology. Rheumatology (Oxford) **56,** 1461, 2017.
18. Bhattaram, P., and Chandrasekharan, U. The joint synovium: a critical determinant of articular cartilage fate in inflammatory joint diseases. Semin Cell Dev Biol **62,** 86, 2017.
19. Myers, S.L., Brandt, K.D., and Eilam, O. Even low-grade synovitis significantly accelerates the clearance of protein from the canine knee: implications for measurement of synovial fluid ''markers'' of osteoarthritis. Arthritis Rheum **38,** 1085, 1995.
20. Levick, J.R., and McDonald, J.N. Fluid movement across synovium in healthy joints: role of synovial fluid macromolecules. Ann Rheum Dis **54,** 417, 1995.
21. Levick, J.R., and McDonald, J.N. Ultrastructure of transport pathways in stressed synovium of the knee in anaesthetized rabbits. J Physiol **419,** 493, 1989.
22. Levick, J.R., Mason, R.M., Coleman, P.J., and Scott, D. Physiology of synovial fluid and trans-synovial flow. In: Archer, C.W., Benjamin, M., Caterson, B., and Ralphs, J.R., eds. The Biology of the Synovial Joint. London: Harwood Academic Publishers, 1999, pp. 235–252.
23. McNamara, L.E., McMurray, R.J., Biggs, M.J.P., Kantawong, F., Oreffo, R.O.C., and Dalby, M.J. Nanotopographical control of stem cell differentiation. J Tissue Eng **2010,** 120623, 2010.

24. Labens, R., Lascelles, B.D.X., Charlton, A.N., *et al*. Ex vivo effect of gold nanoparticles on porcine synovial membrane. Tissue Barriers **1,** e24314, 2013.
25. Fichadiya, A., Bertram, K.L., Ren, G., Yates, R.M., and Krawetz, R.J. Characterizing heterogeneity in the response of synovial mesenchymal progenitor cells to synovial macrophages in normal individuals and patients with osteoarthritis. J Inflamm (Lond) **13,** 12, 2016.
26. Lee, D.M., Kiener, H.P., Agarwal, S.K., *et al*. Cadherin-11 in synovial lining formation and pathology in arthritis. Science **315,** 1006, 2007.
27. Jay, G.D. Characterization of a bovine synovial fluid lubricating factor. I. Chemical, surface activity and lubricating properties. Connect Tissue Res **28,** 71, 1992.
28. Jay, G.D., Torres, J.R., Rhee, D.K., *et al*. Association between friction and wear in diarthrodial joints lacking lubricin. Arthritis Rheum **56,** 3662, 2007.
29. Jay, G.D., Britt, D.E., and Cha, C.J. Lubricin is a product of megakaryocyte stimulating factor gene expression by human synovial fibroblasts. J Rheumatol **27,** 594, 2000.
30. Blasioli, D.J., Matthews, G.L., and Kaplan, D.L. The degradation of chondrogenic pellets using cocultures of synovial fibroblasts and U937 cells. Biomaterials **35,** 1185, 2014.
31. Mitani, G., Sato, M., Yamato, M., *et al*. Potential utility of cell sheets derived from the anterior cruciate ligament and synovium fabricated in temperature-responsive culture dishes. J Biomed Mater Res A **102,** 2927, 2014.
32. Pretzel, D., Pohlers, D., Weinert, S., and Kinne, R.W. In vitro model for the analysis of synovial fibroblast-mediated degradation of intact cartilage. Arthritis Res Ther **11,** R25, 2009.
33. Peck, Y., Leom, L.T., Low, P.F.P., and Wang, D.A. Establishment of an in vitro three-dimensional model for cartilage damage in rheumatoid arthritis. J Tissue Eng Regen Med **12,** e237, 2018.
34. Warnock, J.J., Baker, L., Ballard, G.A., and Ott, J. In vitro synthesis of tensioned synoviocyte bioscaffolds for meniscal fibrocartilage tissue engineering. BMC Vet Res **9,** 242, 2013.
35. Warnock, J.J., Bobe, G., Duesterdieck-Zellmer, K.F., *et al*. Growth factor treated tensioned synoviocyte neotissues: towards meniscal bioscaffold tissue engineering. Vet J **200,** 22, 2014.
36. Kiener, H.P., and Brenner, M.B. Building the synovium: cadherin-11 mediates fibroblast-like synoviocyte cell-to-cell adhesion. Arthritis Res Ther **7,** 49, 2005.
37. Pettipher, E.R., Higgs, G.A., and Henderson, B. Interleukin 1 induces leukocyte infiltration and cartilage proteoglycan degradation in the synovial joint. Proc Natl Acad Sci U S A **83,** 8749, 1986.
38. Tyler, J.A. Insulin-like growth factor 1 can decrease degradation and promote synthesis of proteoglycan in cartilage exposed to cytokines. Biochem J **260,** 543, 1989.
39. Roach, B.L., Kelmendi-Doko, A., Balutis, E.C., Marra, K.G., Ateshian, G.A., and Hung, C.T. Dexamethasone release from within engineered cartilage as a chondroprotective strategy against interleukin-1α. Tissue Eng Part A **22,** 621, 2016.
40. Sampat, S.R., O'Connell, G.D., Fong, J.V., Alegre-Aguarón, E., Ateshian, G.A., and Hung, C.T. Growth factor priming of synovium-derived stem cells for cartilage tissue engineering. Tissue Eng Part A **17,** 2259, 2011.
41. Alegre-Aguarón, E., Sampat, S.R., Xiong, J.C., *et al*. Growth factor priming differentially modulates components of the extracellular matrix proteome in chondrocytes and synovium-derived stem cells. PLoS One **9,** e88053, 2014.
42. Tan, A.R., Alegre-Aguarón, E., O'Connell, G.D., *et al*. Passage-dependent relationship between mesenchymal stem cell mobilization and chondrogenic potential. Osteoarthritis Cartilage **23,** 319, 2015.
43. Lima, E.G., Tan, A.R., Tai, T., *et al*. Differences in interleukin-1 response between engineered and native cartilage. Tissue Eng Part A **14,** 1721, 2008.
44. Kuroki, K., Stoker, A.M., and Cook, J.L. Effects of proinflammatory cytokines on canine articular chondrocytes in a three-dimensional culture. Am J Vet Res **66,** 1187, 2005.
45. Riesle, J., Hollander, A.P., Langer, R., Freed, L.E., and Vunjak-Novakovic, G. Collagen in tissue-engineered cartilage: types, structure, and crosslinks. J Cell Biochem **71,** 313, 1998.
46. Hollander, A.P., Heathfield, T.F., Webber, C., *et al*. Increased damage to type II collagen in osteoarthritic articular cartilage detected by a new immunoassay. J Clin Invest **93,** 1722, 1994.
47. Lee, H.G., and Cowman, M.K. An agarose gel electrophoretic method for analysis of hyaluronan molecular weight distribution. Anal Biochem **219,** 278, 1994.
48. Zimmermann, T., Kunisch, E., Pfeiffer, R., *et al*. Isolation and characterization of rheumatoid arthritis synovial fibroblasts from primary culture—primary culture cells markedly differ from fourth-passage cells. Arthritis Res **3,** 72, 2001.
49. Yuan, S.Y., and Rigor, R.R. Methods for Measuring Permeability. Morgan and Claypool Life Sciences, San Rafaelm, CA, 2010.
50. Garcia, A.N., Vogel, S.M., Komarova, Y.A., and Malik, A.B. Permeability of endothelial barrier: cell culture and *in vivo* models. In: Turksen, K., ed. Permeability Barrier. Humana Press, New York, 2011, pp. 333–354.
51. Gonçalves, R., and Mosser, D.M. The isolation and characterization of murine macrophages. Current Protocols in Immunology. John Wiley and Sons, Inc., Hoboken, NJ, 2001.
52. Cook, J.L., Kuroki, K., Stoker, A., Streppa, H., and Fox D.B. Review of *in vitro* models and development and initial validation of a novel co-culture model for the study of osteoarthritis. Curr Rheumatol Rev **3**, 172, 2007.
53. Lee, J.H., Fitzgerald, J.B., DiMicco, M.A., *et al*. Co-culture of mechanically injured cartilage with joint capsule tissue alters chondrocyte expression patterns and increases ADAMTS5 production. Arch Biochem Biophys **489,** 118, 2009.
54. Jiang, D., Liang, J., and Noble, P.W. Hyaluronan as an immune regulator in human diseases. Physiol Rev **91,** 221, 2011.
55. Stern, R. Hyaluronan catabolism: a new metabolic pathway. Eur J Cell Biol **83,** 317, 2004.
56. Hardy, M.M., Seibert, K., Manning, P.T., *et al*. Cyclooxygenase 2-dependent prostaglandin E2 modulates cartilage proteoglycan degradation in human osteoarthritis explants. Arthritis Rheum **46,** 1789, 2002.
57. Beekhuizen, M., Bastiaansen-Jenniskens, Y.M., Koevoet, W., *et al*. Osteoarthritic synovial tissue inhibition of proteoglycan production in human osteoarthritic knee cartilage: establishment and characterization of a long-term cartilage-synovium coculture. Arthritis Rheum **63,** 1918, 2011.

58. Swärd, P., Wang, Y., Hansson, M., Lohmander, L.S., Grodzinsky, A.J., and Struglics, A. Coculture of bovine cartilage with synovium and fibrous joint capsule increases aggrecanase and matrix metalloproteinase activity. Arthritis Res Ther **19,** 157, 2017.
59. van Buul, G.M., Villafuertes, E., Bos, P.K., *et al*. Mesenchymal stem cells secrete factors that inhibit inflammatory processes in short-term osteoarthritic synovium and cartilage explant culture. Osteoarthritis Cartilage **20,** 1186, 2012.
60. Reyes, L.I., León, F., González, P., *et al*. Dexamethasone inhibits BAFF expression in fibroblast-like synoviocytes from patients with rheumatoid arthritis. Cytokine **42,** 170, 2008.
61. Elsaid, K.A., Fleming, B.C., Oksendahl, H.L., *et al*. Decreased lubricin concentrations and markers of joint inflammation in the synovial fluid of patients with anterior cruciate ligament injury. Arthritis Rheum **58,** 1707, 2008.
62. Sellam, J., and Berenbaum, F. The role of synovitis in pathophysiology and clinical symptoms of osteoarthritis. Nat Rev Rheumatol **6,** 625, 2010.
63. Gitter, B.D., Labus, J.M., Lees, S.L., and Scheetz, M.E. Characteristics of human synovial fibroblast activation by IL-1 beta and TNF alpha. Immunology **66,** 196, 1989.
64. Hamilton, J.A., Butler, D.M., and Stanton, H. Cytokine interactions promoting DNA synthesis in human synovial fibroblasts. J Rheumatol **21,** 797, 1994.
65. Furuzawa-Carballeda, J., Macip-Rodríguez, P.M., and Cabral, A.R. Osteoarthritis and rheumatoid arthritis pannus have similar qualitative metabolic characteristics and pro-inflammatory cytokine response. Clin Exp Rheumatol **26,** 554, 2008.
66. Pulkki, K. The effects of synovial fluid macrophages and interleukin-1 on hyaluronic acid synthesis by normal synovial fibroblasts. Rheumatol Int **6,** 121, 1986.
67. Blewis, M.E., Nugent-Derfus, G.E., Schmidt, T.A., Schumacher, B.L., and Sah, R.L. A model of synovial fluid lubricant composition in normal and injured joints. Eur Cells Mater **13,** 26, 2007.
68. Sabaratnam, S., Arunan, V., Coleman, P.J., Mason, R.M., and Levick, J.R. Size selectivity of hyaluronan molecular sieving by extracellular matrix in rabbit synovial joints. J Physiol **567,** 569, 2005.
69. Coleman, P.J., Scott, D., Mason, R.M., and Levick, J.R. Role of hyaluronan chain length in buffering interstitial flow across synovium in rabbits. J Physiol **526,** 425, 2000.
70. Fraser, J.R.E., Kimpton, W.G., Pierscionek, B.K., and Cahill, R.N.P. The kinetics of hyaluronan in normal and acutely inflamed synovial joints: observations with experimental arthritis in sheep. Semin Arthritis Rheum **22,** 9, 1993.
71. Coleman, P.J., Scott, D., Ray, J., Mason, R.M., and Levick, J.R. Hyaluronan secretion into the synovial cavity of rabbit knees and comparison with albumin turnover. J Physiol **503,** 645, 1997.
72. Marks, P.H., and Donaldson, M.L.C. Inflammatory cytokine profiles associated with chondral damage in the anterior cruciate ligament–deficient knee. Arthroscopy **21,** 1342, 2005.
73. Mwangi, T.K., Berke, I.M., Nieves, E.H., Bell, R.D., Adams, S.B., and Setton, L.A. Intra-articular clearance of labeled dextrans from naive and arthritic rat knee joints. J Control Release **283,** 76, 2018.
74. Utomo, L., van Osch, G.J.V.M., Bayon, Y., Verhaar, J.A.N., and Bastiaansen-Jenniskens, Y.M. Guiding synovial inflammation by macrophage phenotype modulation: an in vitro study towards a therapy for osteoarthritis. Osteoarthritis Cartilage **24,** 1629, 2016.
75. O'Brien, K., Tailor, P., Leonard, C., *et al*. Enumeration and localization of mesenchymal progenitor cells and macrophages in synovium from normal individuals and patients with pre-osteoarthritis or clinically diagnosed osteoarthritis. Int J Mol Sci **18,** 774, 2017.
76. Sugawara, S., Sugiyama, A., Nemoto, E., Rikiishi, H., and Takada, H. Heterogeneous expression and release of CD14 by human gingival fibroblasts: characterization and CD14-mediated interleukin-8 secretion in response to lipopolysaccharide. Infect Immun **66,** 3043, 1998.
77. Manferdini, C., Paolella, F., Gabusi, E., *et al*. Adipose stromal cells mediated switching of the pro-inflammatory profile of M1-like macrophages is facilitated by PGE2: in vitro evaluation. Osteoarthritis Cartilage **25,** 1161, 2017.
78. Fell, H.B. Synoviocytes. J Clin Pathol Suppl (R Coll Pathol) **12,** 14, 1978.
79. Graabaek, P.M. Characteristics of the two types of synoviocytes in rat synovial membrane. An ultrastructural study. Lab Invest **50,** 690, 1984.

Address correspondence to:
Clark T. Hung, PhD
351 Engineering Terrace Building
1210 Amsterdam Avenue
Mail Code 8904
New York, NY 10027

E-mail: cth6@columbia.edu

Received: May 22, 2018
Accepted: August 31, 2018
Online Publication Date: October 30, 2018